

On the dynamics of tilted black hole-torus systems

Vassilios Mewes^{1*}, Filippo Galeazzi², José A. Font^{1,3}, Pedro J. Montero⁴,
and Nikolaos Stergioulas⁵

¹*Departamento de Astronomía y Astrofísica, Universidad de Valencia, 46100 Burjassot (Valencia), Spain*

²*Lehrter Straße 51 HH, 10557 Berlin, Germany*

³*Observatori Astronòmic, Universitat de València, C/ Catedrático José Beltrán 2, 46980, Paterna (València), Spain*

⁴*Max-Planck-Institut für Astrophysik, Karl-Schwarzschild-Str. 1, 85741 Garching, Germany*

⁵*Department of Physics, Aristotle University of Thessaloniki, Thessaloniki 54124, Greece*

29 March 2022

ABSTRACT

We present results from three-dimensional, numerical relativity simulations of a *tilted* black hole-thick accretion disc system. The simulations are analysed using tracer particles in the disc which are advected with the flow. Such tracers, which we employ in these new simulations for the first time, provide a powerful means to analyse in detail the complex dynamics of tilted black hole-torus systems. We show how its use helps to gain insight in the overall dynamics of the system, discussing the origin of the observed black hole precession and the development of a global non-axisymmetric $m = 1$ mode in the disc. Our three-dimensional simulations show the presence of quasi-periodic oscillations (QPOs) in the instantaneous accretion rate, with frequencies in a range compatible with those observed in low mass X-ray binaries with either a black hole or a neutron star component. The frequency ratio of the dominant low frequency peak and the first overtone is $\omega_1/f \sim 1.9$, a frequency ratio not attainable when modelling the QPOs as p -mode oscillations in axisymmetric tori.

Key words: accretion, accretion discs – black hole physics – hydrodynamics – instabilities – X-rays: binaries

1 INTRODUCTION

The majority of accretion discs around Kerr black holes (BH) is believed to be tilted with respect to the equatorial plane of the central BH (see [Fragile et al. \(2001\)](#); [Maccarone \(2002\)](#); [Fragile et al. \(2007\)](#) for arguments). Recent fully general relativistic hydrodynamics (GRHD) simulations of tilted black hole-neutron star (BHNS) mergers have shown that a tilted, thick accretion disc can self-consistently form in these events ([Foucart et al. 2011, 2013](#); [Kawaguchi et al. 2015](#)). In a tilted BH–torus system, the dynamics of the system is fundamentally different from the aligned case due to general relativistic effects affecting inclined particle orbits in the Kerr spacetime, such as the Lense–Thirring (LT) effect ([Lense & Thirring 1918](#)). The torque caused by the LT effect has a strong radial (r^{-3}) dependence and causes the disc to start precessing differentially, as a result of which it might become *twisted* and *warped*, affecting its dynamical behaviour (see [Nelson & Papaloizou \(2000\)](#) for a definition of twist and warp). In thick, tilted discs around Kerr BHs,

the evolution and propagation of warps can be described by bending waves rather than diffusion ([Ivanov & Illarionov 1997](#); [Demianski & Ivanov 1997](#); [Lubow et al. 2002](#)). In particular, in these systems the tilt angle does not approach zero in the vicinity of the central BH, as one would expect if the viscous Bardeen–Petterson effect ([Bardeen & Petterson 1975](#)) would be at play. This behaviour of the radial tilt profile in the inner region of thick, tilted accretion discs has been observed in the inviscid GRHD simulations of [Fragile & Anninos \(2005\)](#), which were performed in a fixed background metric, as well as in our recent fully dynamical GRHD simulations ([Mewes et al. 2016](#)), hereafter referred to as Paper I. Incorporating general relativistic effects in the simulations of these systems is necessary to obtain correct disc evolutions, see for instance [Nealon et al. \(2016\)](#), where omitting or incorporating general relativistic apsidal precession completely changes the evolution of the tilt angle in the vicinity of the central BH.

In geometrically thick and radially slender discs such as the ones studied in [Fragile & Anninos \(2005\)](#) and Paper I, the response of the disc to the LT torque is solid body precession, as the sound crossing time of the disc is much shorter

* E-mail: vassilios.mewes@uv.es

than the LT timescale (Fragile & Anninos 2005). The precessing disc is exerting an equal and opposite torque on the central Kerr BH (King et al. 2005), which should therefore start to precess as well, at least in those systems in which the disc mass is not negligible and the spacetime therefore cannot be assumed to be a fixed background. In Paper I we indeed observed significant precession of the central Kerr BH for all models we studied. As described by King et al. (2005), the LT torque alone does not act in a direction that results in disc alignment. However, there have been early arguments that the central BH should eventually align with the disc angular momentum (Rees 1978; Scheuer & Feiler 1996). In particular King et al. (2005) argued that the total torque cannot have a component in the direction of the BH spin, but can be broken down to a contribution that induces precession and a second, dissipative torque that tends to align the BH and the accretion disc. Recently, in the post-merger phase of the BHNS merger simulations of Kawaguchi et al. (2015), the authors found a significant alignment of the accretion disc in a timescale compared to the accretion timescale of the disc. These authors suspected that the alignment could have been due to the transport of angular momentum induced by non-axisymmetric shock waves in the disc. In Paper I, we also observed phases of significant alignment, particularly during the growth of a global, non-axisymmetric instability in some of our disc models, which we identified as the Papaloizou-Pringle instability (PPI) (Papaloizou & Pringle 1984).

In this paper we revisit in detail one of the models we studied in Paper I, model NC1a03b05, performing two new simulations of a tilted black hole-torus system, one with the spacetime fully evolved and a second one keeping the spacetime fixed (i.e. in the so-called Cowling approximation). In these new simulations we use fluid tracers placed in the disc at the beginning of the simulation that are advected with the flow. Such tracers provide an additional valuable means to analyse the disc evolution. In performing these new simulations and analysing the disc evolution in greater detail, we gain insight on the origin of the observed BH precession as well as in the development of the observed global non-axisymmetric $m = 1$ mode in the disc and the resulting dynamics of the system. Non-axisymmetric $m = 1$ modes are special in that, once they appear, the centre of mass of the disc does not coincide with the centre of mass of the system anymore, leading to a perturbed potential that causes a drift of the central mass away from the centre of mass of the system (Adams et al. 1989; Heemskerk et al. 1992). The induced motion of the central mass can also enhance the strength of the $m = 1$ mode significantly (Adams et al. 1989; Christodoulou & Narayan 1992).

Furthermore, the growth of the $m = 1$ mode modulates the instantaneous accretion rate, a quantity which is commonly employed as a measure of X-ray luminosity (van Paradijs et al. 1988; Méndez et al. 1999). The presence of quasi-periodic oscillations (QPOs) in the accretion rate and their association with the disc evolution has been used to explain the QPOs observed in low mass X-ray binaries (LMXBs) (see e.g. van der Klis (2006) and references therein). Here, we show that QPOs are indeed present in the accretion rate and that their frequencies are in a range compatible with those observed in LMXBs.

This paper is organised as follows: We briefly describe

the simulation details and the properties of the initial model in Section 2. Our results are presented and discussed in detail in Sections 3.1 and 3.2. Finally, we present our conclusions in Section 4. Unless specific units are given, throughout this paper we employ geometrised units $c = G = M_\odot = 1$ where c , G and M_\odot are the speed of light, the gravitational constant and the solar mass, respectively.

2 COMPUTATIONAL FRAMEWORK

The simulations reported in this paper use the same numerical relativity codes and techniques used for the simulations of Paper I. We briefly summarise here the basic ingredients, addressing the interested reader to Paper I for details. The simulations are performed with the Einstein Toolkit (Löffler et al. 2012), an open source, numerical relativity code that solves the Einstein equations in the $3 + 1$ formalism. The spacetime evolution is done with the McLachlan code (Brown et al. 2009; Reisswig et al. 2011), an implementation of the Baumgarte-Shapiro-Shibata-Nakamura (BSSN) formulation (Shibata & Nakamura 1995; Baumgarte & Shapiro 1998), while the hydrodynamics evolution is performed by the GRHydro code (Baiotti et al. 2005; Löffler et al. 2012; Mösta et al. 2014). The computational domain is composed of 13 nested mesh refinement levels, provided by the Carpet code (Schnetter et al. 2004). For the current simulations, the only technical difference lies in the evolution of the spacetime shift vector β^i . While in the study performed in Paper I we used the dynamical η -damping described in Alic et al. (2010), in the current simulations we use the standard Γ -driver shift condition (Alcubierre et al. 2003) (see Löffler et al. (2012) for the implementation details in the Einstein Toolkit). This is motivated by the greater compatibility with the standard version of McLachlan and also in order to check for the influence of the gauge evolution on the physics we observed in Paper I.

The initial model for the current simulations is model NC1a03b05 of Paper I, which has a non-constant specific angular momentum profile and was shown to exhibit the development of a long-lasting non-axisymmetric $m = 1$ mode. The parameters of this model are given in Table 1. We evolve the model up to 32 orbital periods in two different ways in order to gauge the influence of the self-gravity of the fluid in the evolution of this model. The first evolution takes into account the solution of the coupled system of Einstein equations and GRHD equations, and thus corresponds to a fully dynamical spacetime evolution. For the second evolution we assume the test-fluid (Cowling) approximation in which the spacetime is fixed and only the GRHD equations are solved. As initial data for this second simulation we use the data of the fully evolved spacetime run at $t = 1.5t_{\text{orb}}$. This is to ensure that we evolve the same system, and in particular to provide the same perturbation that triggers the growth of the non-axisymmetric instability in both runs.

In order to compute the evolution of the tracer particles in our system, we adopt a simple test particle approximation to convert from the Eulerian representation of the fluid flow (in which the hydrodynamics variables are evolved on the computational grid) to the Lagrangian one, needed to compute the velocity of the particles. This method is often used in the context of core-collapse supernovae simulations

Table 1. Main characteristics of the initial model NC1a03b05. From left to right the columns indicate the central BH mass M_{BH} , the disc-to-BH mass ratio q , defined as the ratio of the total gravitational mass of the torus and the irreducible mass of the BH, the inner and outer disc radii r_{in} and r_{out} , the maximum rest-mass density ρ_c , the polytropic constant K of the equation of state, the orbital period P_{orb} and orbital frequency f_{orb} at the radius of the initial ρ_c , the specific angular momentum profile in the equatorial plane of the disc l (in terms of the Schwarzschild radial coordinate R), the BH spin parameter a , and the initial tilt angle β_0 . The model is evolved with a Γ -law ideal fluid EOS with $\Gamma = 4/3$.

M_{BH}	q	r_{in}	r_{out}	ρ_c	K	P_{orb} [ms]	f_{orb} [Hz]	l -profile	a	β_0
0.9775	0.110	3.60	33.5	1.69×10^{-5}	0.170	1.19	843	$3.04 R^{0.11}$	0.3	5

to describe the evolution of the unbound matter subject to r-process nucleosynthesis (see Travaglio et al. (2004); Nakamura et al. (2015)). These passively advected particles allow us to record their velocity, internal energy and pressure by interpolating the corresponding quantities from the underlying grid. We adopt a linear interpolation to project the physical quantities computed on the grid onto the tracer particles.

Using the local 3-velocity of the fluid, \mathbf{v} , lapse function α , and shift vector β we can evolve the position of the particle by simply integrating

$$\frac{d\mathbf{x}}{dt} = \tilde{\mathbf{v}}(\mathbf{x}), \quad (1)$$

where $\tilde{\mathbf{v}} \equiv \alpha\mathbf{v} - \beta$ is the advection speed with respect to the coordinates (Foucart et al. 2014). For the time evolution of the tracers, we use a second-order accurate in time Adams-Bashforth explicit integrator, which requires two previous time steps, t^{n-1} and t^n , to compute the position vector, \mathbf{x} , of the particles at t^{n+1} . As a result, we can express the evolution equation for the position as

$$\mathbf{x}^{n+1} = \mathbf{x}^n + \frac{3}{2}\Delta t (\tilde{\mathbf{v}}^n - \tilde{\mathbf{v}}^{n-1}), \quad (2)$$

where Δt represents the time step relative to the finest mesh refinement where the tracer particle is located.

Initially we place 250000 tracers at random locations according to the underlying rest-mass density ρ distribution in the accretion disc, resulting in all tracer particles being of equal mass (3.97×10^{-7}) initially and during the evolution. The bulk motion of the tracers is able to capture accurately the motion of the underlying fluid flow especially when the fluid flow is not turbulent and strong shocks are not present.

Using this prescription, the tracers are then advected with the fluid flow during the evolution of the disc. The tracers are output in hdf5 snapshots at user-specified time intervals during the evolution, which allows one to perform the disc analysis as a post-processing step rather than during the simulation. The analysis of the disc via the tracer particles performs very well in the bulk regions of the disc and accurately reflect the total mass, energy and angular momentum of the disc during the evolution. For the analysis of complicated flow details in low density regions (such as the accretion streams observed in Fragile & Anninos (2005) and in Paper I), however, the disc analysis thorn described in Paper I performs much more accurate as it analyses the disc morphology using the full 3D data during the evolution. Due to the much larger output files resulting from the output of the 3D spacetime and hydrodynamics variables, the disc analysis has to be performed during the simulation rather than as a post-processing step. Depending on the number of

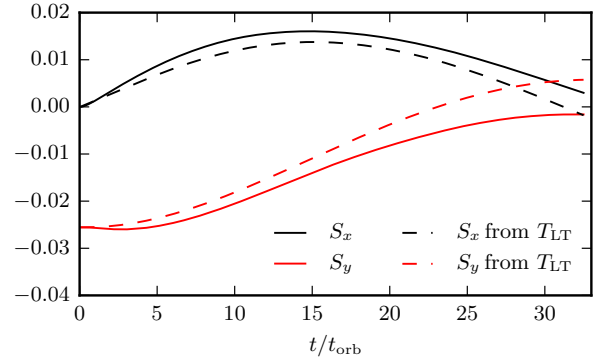


Figure 1. Evolution of the x and y components of the BH spin \mathbf{S} and the evolution of the spin components resulting from the LT torque exerted by the disc.

tracers, it might be computationally cheaper to advect the tracer particles with the flow and later analyse them rather than performing the complicated disc analysis during the simulation. This may significantly reduce the runtime of the evolution simulations. Due to the manageable file sizes of the tracer output, the tracers are furthermore a very powerful tool for the visualisation of the disc evolution.

3 RESULTS

3.1 Black hole precession from Lense-Thirring torque

The main driver of the tilted disc evolution is the Lense-Thirring (LT) precession. At the lowest post-Newtonian order of spin-orbit interactions, a particle in an inclined orbit around a central Kerr BH will be subject to the following torque (Kidder 1995; Merritt & Vasiliev 2012):

$$\mathbf{T}_{\text{LT}} = 2 \frac{\mathbf{S} \times \mathbf{J}}{r^3}, \quad (3)$$

where \mathbf{S} is the BH spin, \mathbf{J} is the angular momentum vector of the particle, and r is the distance of the particle from the BH centre. This is the LT torque exerted by the central BH on the particle. As a result of this torque, the orbital angular momentum of the particle will start to precess around the BH spin. As there is a strong radial dependence on the magnitude of the torque, the inner regions of a tilted accretion disc will become twisted, i.e. they will differentially precess around the central BH. However, as shown in the results of Fragile & Anninos (2005) and in Paper I, the sound crossing time in the disc is shorter than the LT timescale,

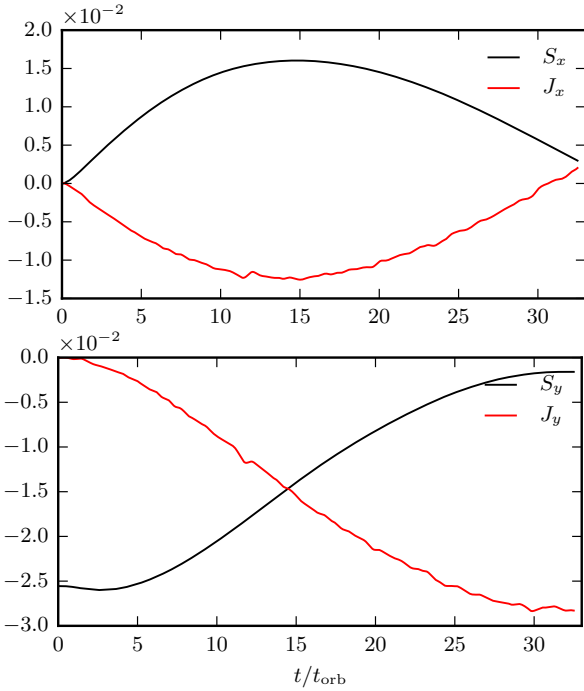


Figure 2. Evolution of the x and y components of the BH spin \mathbf{S} and total disc angular momentum \mathbf{J}_{disc} .

which results in a global disc response to the LT torque produced by the Kerr BH, leading to solid body precession of the disc. The disc exerts a torque of equal magnitude and opposite direction on the BH, causing it to precess as well.

To check whether the precession of the BH we observe in our simulations has a physical origin, we compare the time evolution of the x and y components of the BH spin, S_x, S_y , with the evolution of the BH spin that would have resulted from summing up the cumulative spin change resulting from the LT torque of the disc at each timestep:

$$\mathbf{S}_{\text{LT}}(t) = \mathbf{S}(0) + \int_0^t \mathbf{T}_{\text{LT}} dt. \quad (4)$$

As the disc is approximately precessing as a solid body, we calculate the torque coming from the disc total angular momentum vector, \mathbf{J}_{disc} , choosing a radius of $r = 15.0$ in Eq. (3). The results are shown in Figure 1. This figure shows that the time evolution of the BH spin components agree well with the torque exerted on the BH by the disc. In Fig. 2 we show the time evolution of the x and y components of \mathbf{S} and \mathbf{J}_{disc} . Clearly, the sum of the spin components and disc angular momentum components along the two directions is seen to be approximately constant for the evolution, in agreement with the fact that the LT torque is the main driver for both disc and BH precession.

3.2 $m = 1$ non-axisymmetric instability

3.2.1 Spiral density wave

Two of the three models we studied in Paper I were found to develop a global non-axisymmetric instability with $m = 1$ being the dominant azimuthal mode. One such instability is the instability of tori with constant specific angular momentum profiles, the Papaloizou-Pringle instability (Papaloizou

& Pringle 1984). Early numerical investigations of Hawley (1987) showed that the non-linear regime of the PPI resulted in the formation of counterrotating overdensity lumps, which were dubbed ‘planets’. The precise mechanism of the instability was elucidated by Goodman et al. (1987) who showed that the planets found in Hawley (1987) might be a new equilibrium configuration of the fluid. The instability was subsequently investigated numerically by Hawley (1991) as well as in the recent, fully general relativistic simulations of Korobkin et al. (2011); Kiuchi et al. (2011) and those presented in Paper I.

We note here that the role played by magnetic fields in connection with non-axisymmetric hydrodynamical instabilities such as the PPI is not yet fully understood. The interest in the PPI quickly diminished after the discovery that the magneto-rotational instability (MRI) (Velikhov 1959; Chandrasekhar 1960) is active in accretion discs (Balbus & Hawley 1991), because accretion has been seen to effectively stabilise a disc against the development of the PPI (Blaes 1987). However, Fu & Lai (2011) suggest that highly magnetised tori might still be unstable to global hydrodynamic instabilities. We plan on studying the effects played by magnetic fields on the development and growth of global non-axisymmetric instabilities through numerical relativity simulations of magnetised accretion tori around BHs in future work.

In this section we show that the growth of the $m = 1$ mode in the disc results in the formation of a spiral density wave with a constant global pattern speed Ω_P . As the disc is differentially rotating this means that there is a location in the disc, the so-called corotation radius r_{co} , where the spiral density wave has the same orbital velocity as the fluid in the disc. Inside r_{co} the wave travels slower than the fluid, which means that it has negative angular momentum with respect to the fluid. While the wave amplitude is linear, it does not interact with the fluid, but once non-linear amplitude effects come into play, the spiral density wave can couple to the fluid via dissipation (Papaloizou & Lin 1995; Goodman & Rafikov 2001; Heinemann & Papaloizou 2012). When this happens, the wave begins to transport angular momentum outwards as the fluid loses angular momentum to the wave inside the corotation radius. The development and persistence of the spiral density wave is shown in Figure 3. The figure shows the fractional change in density between two successive snapshots $\Delta\rho/\rho$ at 9 different times of the disc evolution, as well as the tracer particles that are located at r_{co} (grey circles). The location of the corotation radius is defined as the radius where the $m = 1$ pattern speed and the fluid orbital velocity are equal. As usual, the non-axisymmetric modes in the disc are analysed by means of an azimuthal Fourier transform of the rest-mass density ρ (Zurek & Benz 1986; Heemskerk et al. 1992):

$$D_m = \int \alpha \sqrt{\gamma} \rho e^{-i m \phi} d^3 x, \quad (5)$$

with α and γ being the spacetime lapse function and the determinant of the 3-dimensional metric, respectively. Similarly, the mode analysis performed using the tracers is accomplished by means of the following sum

$$D_m = \sum_j^N m_j e^{-i m \phi}, \quad (6)$$

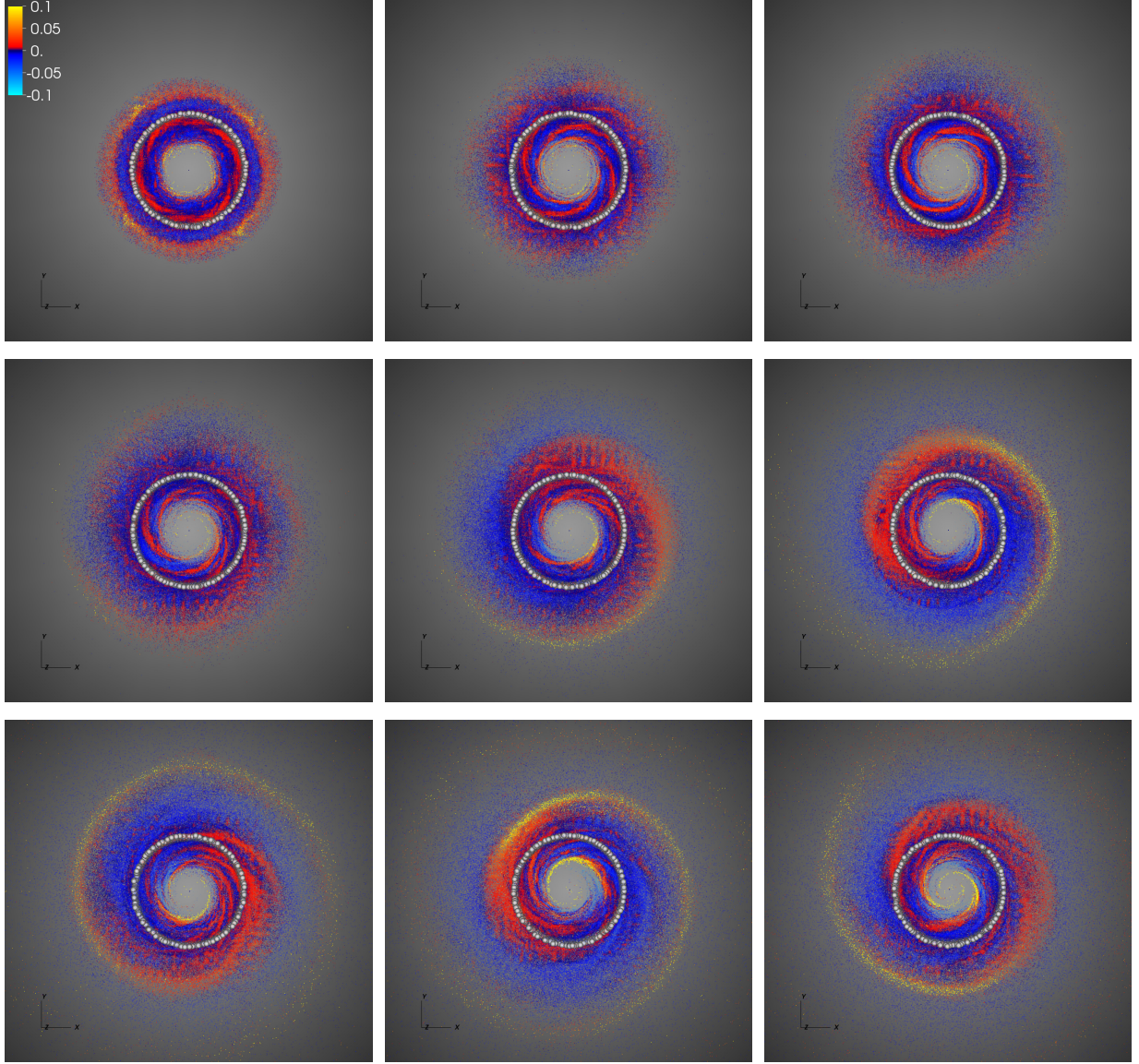


Figure 3. Fractional change in the rest mass density $\Delta\rho/\rho$ between two timesteps, shown at 9 different snapshots of the evolution, $t/t_{\text{orb}} = 1, 4, 8, 12, 16, 20, 24, 28$, and 32 (from the top-left panel). The domain shown in all panels is 100 (~ 148 km) across both axes. The grey circles show the tracers at the location of the corotation radius r_{co} . The formation of a spiral density wave from the growth of the $m = 1$ mode is noticeable.

where m_j is the mass of each tracer particle. From the mode amplitudes, the pattern speed of an azimuthal mode with mode number m is defined as (see, for instance [Heemskerk et al. \(1992\)](#))

$$\Omega_P = \frac{1}{m} \frac{d\phi_m}{dt}, \quad (7)$$

where the phase angle ϕ_m is given by

$$\phi_m = \tan^{-1} \left(\frac{\text{Im}(-D_m)}{\text{Re}(D_m)} \right). \quad (8)$$

For our simulation, we obtain an orbital period of the $m = 1$ pattern of $P_P \sim 1.96$ ms, which is slightly shorter than twice the initial orbital period of the disc at the location of the density maximum (see [Table 1](#)). We note that we have chosen the same range of the fractional change in the

rest-mass density in all snapshots shown in [Figure 3](#), which corresponds to the interval $[-0.1, 0.1]$. At these wave amplitudes, non-linear effects are negligible compared to the linear effects ([Masset & Tagger 1997](#)). This plot range has however been chosen for visualisation purposes and the wave amplitudes are actually much larger than 0.1 after the saturation of the $m = 1$ growth, reaching almost unity. At these wave amplitudes non-linear effects are important and the spiral density wave can couple to the fluid via dissipation. To show the development of weak shocks, we plot the fractional change in the entropy $S = p/\rho^\Gamma$ for tracers with $\Delta\rho/\rho > 0.1$ in [Figure 4](#). From this plot, we clearly see an increase in the fluid entropy in the inner and outer regions of the spiral density wave. In some snapshots of [Figure 3](#), we can see fractional changes in ρ in the form of two spiral arms in the inner regions of the disc. The dominant $m = 1$

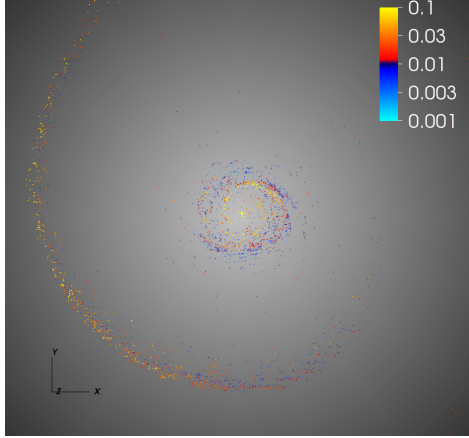


Figure 4. Fractional change in the fluid entropy S between two timesteps, for tracers with $\Delta\rho/\rho > 0.1$, shown at $t/t_{\text{orb}} = 32$.

mode developing in the disc should not produce these, which means there could be a different mechanism at play. Standing shocks in the inner regions of tilted accretion discs in the form of two spiral arms have been observed and analysed in [Henisey et al. \(2012\)](#); [Generozov et al. \(2014\)](#) and are a distinctive feature of tilted accretion discs. Finally, we note that the mesh refinement boundaries of our computational grid also produce entropy changes due to numerical dissipation. However, these changes are about an order of magnitude smaller than the physical increase of entropy due to the development of shocks in the spiral density wave.

3.2.2 Gravitational torque and motion of the central black hole

We next turn to the interaction of the non-axisymmetric $m = 1$ mode and the central BH. The moving overdensity planet in the disc represents a time-changing non-axisymmetric gravitational potential. Following [Roedig et al. \(2012\)](#), we estimate the total gravitational torque on the BH exerted by the fluid is estimated by using the tracer particles at time t in the following way:

$$\mathbf{T}_G(t) = \sum_i^N M_{\text{BH}}(t) m_i \frac{\mathbf{r}_{\text{BH}}(t) \times (\mathbf{r}_i(t) - \mathbf{r}_{\text{BH}}(t))}{|\mathbf{r}_i(t) - \mathbf{r}_{\text{BH}}(t)|^3}, \quad (9)$$

where the sum runs over all tracer particles and the time dependent BH mass $M_{\text{BH}}(t)$ and BH position vector $\mathbf{r}_{\text{BH}}(t)$ are obtained using the `QuasiLocalMeasures` ([Dreyer et al. 2003](#); [Schnetter et al. 2006](#)) and `AHFinderDirect` ([Thornburg 2003](#)) thorns, respectively.

The resulting components of the gravitational torque \mathbf{T}_G and the time derivative of the components of the BH orbital angular momentum $\dot{\mathbf{L}}_{\text{BH}}$, are shown in Figure 5. This figure clearly shows that the orbital angular momentum of the BH is caused by the gravitational torque of the non-axisymmetric matter distribution in the disc. The orbital angular momentum components of the BH are calculated using the flat space coordinate rotational Killing vectors on the apparent horizon (AH) ([Campanelli et al. 2007](#)) (which gives the Komar angular momentum in axisymmetry ([Mewes et al. 2015](#))) without the subtraction of the position of the BH centre and the subsequent subtraction of the

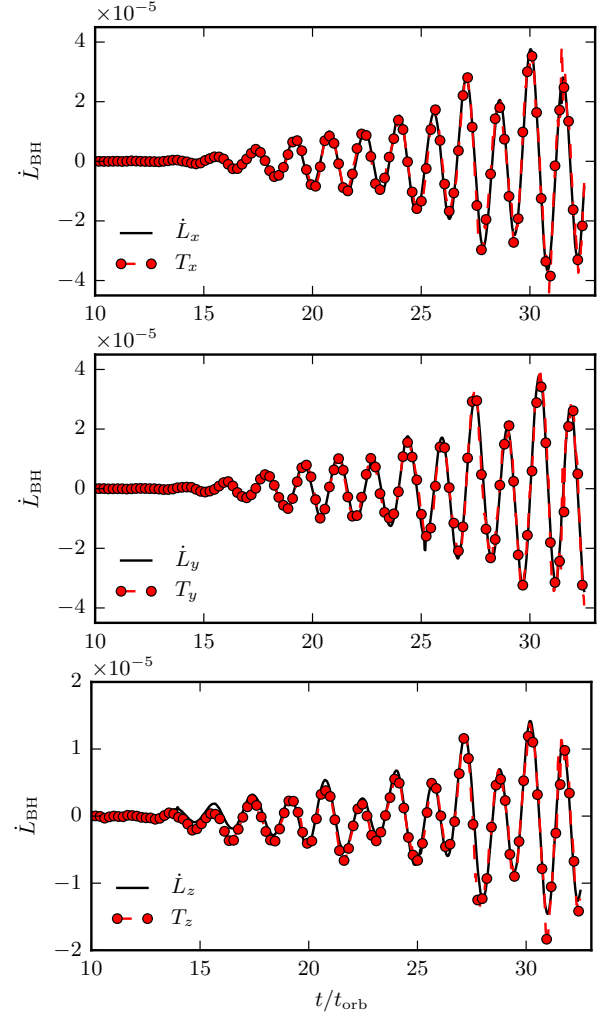


Figure 5. Time derivative of the components of the BH orbital angular momentum vector \mathbf{L}_{BH} and the components of the gravitational torque computed from the non-axisymmetric matter distribution \mathbf{T}_G .

intrinsic spin of the AH. While this is by no means a gauge invariant measure of the orbital angular momentum of the BH, it agrees very well with the Newtonian calculation of the BH orbital angular momentum as

$$\mathbf{L}_{\text{BH}} = M_{\text{BH}} \mathbf{r}_{\text{BH}} \times \mathbf{v}_{\text{BH}}. \quad (10)$$

The disc acquires some bulk orbital angular momentum (equal and opposite to that of the BH) as a result of the growth and the longevity of the $m = 1$ mode as well. During the later stages of the evolution, after the saturation of the $m = 1$ mode growth, this bulk orbital angular momentum of the disc becomes comparable to the fluid angular momentum in the x and y directions. It is precisely the evolution of the bulk orbital angular momentum that we mistakenly identified as tilt and twist oscillations in Paper I. This was due to an error in the reading of the location of the BH centre in the disc analysis code described in Paper I, which ultimately resulted in the calculation of the disc angular momentum about the grid origin rather than about the BH centre.

As a result of this error in the disc analysis used for the

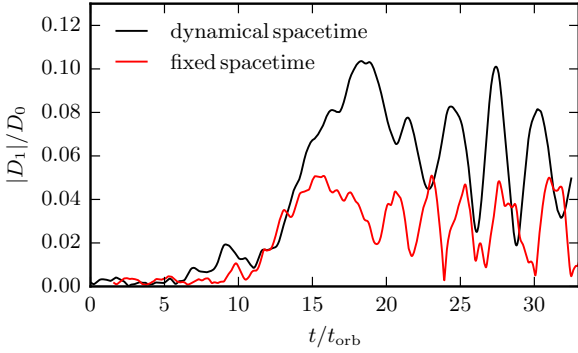


Figure 6. Evolution of the $m = 1$ mode for the dynamical spacetime simulation (black line) and for the fixed spacetime simulation (red curve), calculated with the tracer particles.

results presented in Paper I, we speculated that the observed global oscillations in the tilt and twist might be due to the development of the Kozai-Lidov (KL) effect (Kozai 1962; Lidov 1962). This effect results in the periodic exchange of the inclination and eccentricity of a particle orbit around a central mass that is itself in an orbit with a third mass (the so-called perturber). The effect is a direct consequence of the conservation of the total angular momentum of the system. As the KL effect has recently been observed to operate in inclined hydrodynamical discs around a central mass which is in a binary with another mass (Martin et al. 2014), we assumed in Paper I that the KL effect might be in operation in our discs as the long-lasting $m = 1$ mode forces the central BH to move in a quasi-binary orbit with the overdensity planet in the disc. To demonstrate the operation of the KL effect and to explain the oscillations in more detail has been one of the main motivations for carrying out new simulations and employing the tracer particles as a new tool for the analysis of the disc. As explained above, we have clarified the origin of the global tilt and twist oscillations as being connected to the bulk orbital angular momentum the disc acquires when forming the quasi-binary system with the BH. The KL effect is therefore not seen to be in operation in our discs.

The effect of the motion of the central BH on the strength of the $m = 1$ mode is shown in Figure 6. This figure displays the time evolution of the normalised magnitude of the D_1 mode for our two simulations. While growth rates of the $m = 1$ mode strength are very similar for the two runs, the maximum mode amplitude is about two times higher in the fully dynamical spacetime simulation (where the BH is allowed to move). We note that the growth rate and maximum $m = 1$ mode amplitude in the simulation presented here is smaller than the one reported in Paper I for the same model (the maximum of the $m = 1$ mode amplitude is half of that reported in Paper I). The difference arises from the use of a constant damping parameter in the standard Γ -driver shift condition, which is known to be less accurate than dynamical damping parameters for large mass-ratio binary BH simulations (see for instance Gold & Brügmann (2013)). The dynamics of the high mass-ratio quasi-binary system composed of the central BH and the moving overdensity planet in the disc should therefore be described with better accuracy using the dynamical damping parameter employed in

Paper I. It seems that the fixed damping parameter restricts the BH motion, resulting in a smaller mode power. We note, however, that the actual development of the instability and the overall properties of the disc after its saturation remain unaffected by the choice of gauge, as they should.

3.2.3 Disk alignment

As shown by King et al. (2005), the direction of the torque responsible for disc (and therefore also BH) precession does not act in a direction to align the disc angular momentum with the central BH. The alignment torque ultimately results from the inclusion of the effects of viscosity or dissipation, and its magnitude depends, as King et al. (2005) remark, on the actual disc properties. As our fluid evolution does not explicitly account for viscosity, viscous and dissipative effects might therefore only arise due to numerical viscosity and dissipation in shocks. As we have seen in Section 3.2.1, the spiral density wave that results from the development of the $m = 1$ mode provides dissipation that is stronger than the one arising from the numerics. Another factor working towards alignment of the BH spin and the disc is the accretion of angular momentum, which is a negligible effect in our simulations due to the very low amount of total mass accreted during the evolution.

In Figure 7, we plot a spacetime diagram showing the evolution of the tilt angle profile $\nu(r)$ obtained from the tracers. Similar to the disc analysis explained in Nelson & Papaloizou (2000); Fragile & Anninos (2005) and employed in Paper I, we split the domain in radial shells and calculate the components of the total angular momentum of all tracers within a given shell to obtain the tilt profile. We clearly see the expected, non-zero oscillating tilt profile predicted by the warp propagation as bending waves during the early stages of the simulation. The tilt amplitude close to the central BH is significantly reduced from about $15t_{\text{orb}}$ onwards. This could be connected to the time when the developing spiral density wave becomes non-linear for the first time, coupling to the fluid inside the corotation radius and lowering the tilt amplitude.

We do not see a complete global alignment as observed in Kawaguchi et al. (2015) during the time of the evolution. However, as Figure 8 shows, there is a clear monotonic drop in the global tilt angle ν_{disc} from $t = 2t_{\text{orb}}$ onwards, which is when the $m = 1$ non-axisymmetric mode starts growing. Kawaguchi et al. (2015) noted that the alignment timescale was comparable or shorter than the precession timescale of the disc. We note that our disc is precessing slower than the ones studied in Kawaguchi et al. (2015), as our initial BH spin is much smaller than that of the central BH they obtain in their BHNS merger simulations. In our dynamical spacetime simulation, both the disc angular momentum and BH spin have completed half a precession cycle within $32t_{\text{orb}}$, while the global tilt angle ν_{disc} has not dropped by half within the same period. A difference between our disc evolution and the ones described in Kawaguchi et al. (2015) is the accretion timescale, which in their case is comparable to the precession timescale and, therefore, to the alignment timescale. We do not observe this behaviour in our simulations, as the total rest mass accreted during the evolution (2.6×10^{-3}) is very small compared to the initial disc rest mass (1.02×10^{-1}). Assuming that the accretion rate remains

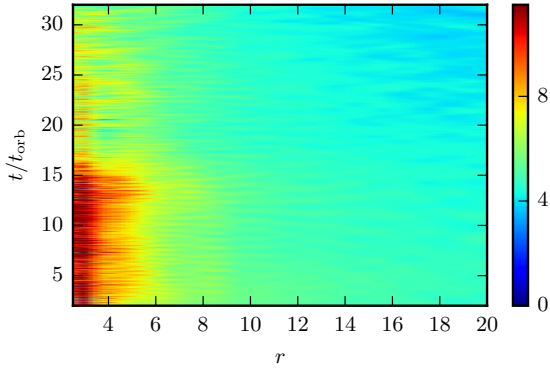


Figure 7. Spacetime diagram of the radial profile of the tilt angle $\nu(r)$. The tilt angle is shown in degrees.

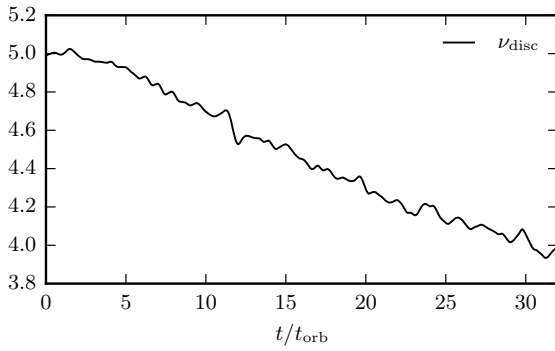


Figure 8. Time evolution of the global tilt angle of the disc, ν_{disc} , shown in degrees.

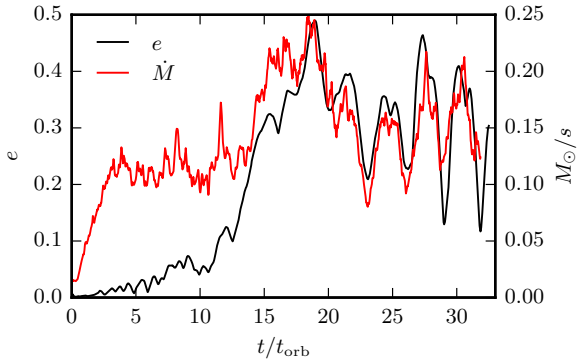


Figure 9. Evolution of the sum of disc eccentricity e_1 and disc ellipticity e_2 and of the rest mass accretion rate \dot{M} in units of M_{\odot}/s . The accretion rate has been shifted by $0.65 t_{\text{orb}}$ in time for a better visualisation of the correlation between its modulation and that of e .

constant for the lifetime of the disc, the accretion timescale would be ~ 10 times larger than the precession timescale of the disc.

3.3 QPOs in the accretion rate

As already observed in Paper I, the growth of the $m = 1$ non-axisymmetric mode in the disc strongly influences the instantaneous accretion rate. As the accretion rate can be

assumed to be a measure of X-ray luminosity (see, for instance [van Paradijs et al. \(1988\)](#); [Méndez et al. \(1999\)](#)), finding QPOs in the accretion rate and correlating them with the disc evolution might serve as a model to explain the QPOs observed in LMXBs (see e.g. [van der Klis \(2006\)](#) and references therein). The origin of these QPOs is still not fully understood, and there are various models trying to explain the observed X-ray variability in these sources (see [Lai & Tsang \(2009\)](#) for a detailed summary of the proposed models, [Belloni & Stella \(2014\)](#) for a recent review of QPOs in LMXBs and [Mishra et al. \(2015\)](#); [Mazur et al. \(2016\)](#) for recent models).

As matter accretion implies the development of a radial flow, we follow [MacFadyen & Milosavljević \(2008\)](#) and calculate the eccentricity e_1 and ellipticity e_2 of the tracer particles as

$$e_n = \frac{|\sum_{j=1}^N m_j v^r e^{in\phi}|}{\sum_{j=1}^N m_j v^\phi}, \quad (11)$$

where v^r and v^ϕ are the radial and azimuthal components of the 3-velocity, respectively. We denote the sum of disc eccentricity and ellipticity by

$$e \equiv e_1 + e_2. \quad (12)$$

The evolution of e together with the mass accretion rate \dot{M} is plotted in Figure 9. As in Paper I, we calculate the accretion rate as the following surface integral at the AH:

$$\dot{M} = 2\pi r^2 \int_0^{2\pi} \int_0^\pi D v^r \sin\theta d\phi d\theta, \quad (13)$$

where $D \equiv \sqrt{\gamma}\rho W$ is the relativistic rest-mass density, and W is the Lorentz factor. The mass accretion rate in Fig. 9 has been shifted by $0.65 t_{\text{orb}}$ to better illustrate that the accretion rate is clearly modulated by e and shows distinct QPOs. As expected, the applied shift is backwards in time, as the evolution of \dot{M} trails the evolution of e . The power spectral densities (PSD) of e , \dot{M} and the radial velocity of the BH are shown in Figure 10. The PSD show a clear dominant peak at ~ 260 Hz with a first overtone at ~ 490 Hz for e and \dot{M} . Note that the frequency of the first overtone is compatible with the orbital frequency of the $m = 1$ pattern, which is ~ 510 Hz. The frequency ratio of the dominant low frequency peak and the overtone is $\omega_1/f \sim 1.9$. The double peak in the PSD arises from the modulation of the strength of the $m = 1$ mode (see Fig. 6). The modulation causes changes in the eccentricity of the orbital motion of the BH as well, which is displayed in Fig. 11.

Periodicity in the accretion rate due to the inner region of a circumbinary accretion disc becoming eccentric has also been observed in [Farris et al. \(2014\)](#), as well as in the MHD simulations of [Machida & Matsumoto \(2008\)](#), where the authors attribute the QPOs in the accretion rate to the development of a $m = 1$ non-axisymmetric mode. We note that the QPO frequencies extracted from our simulation are for a fiducial model with a central BH mass of $\sim 1 M_{\odot}$ (see Table 1). The observed frequencies in these systems usually scale as M^{-1} , where M is the mass of the central compact object, as in the p -mode torus oscillation model of [Rezzolla et al. \(2003\)](#). Assuming the M^{-1} frequency scaling to be universal (see for instance [Abramowicz et al. \(2004\)](#); [Zhou et al. \(2015\)](#) for arguments and observational support), this

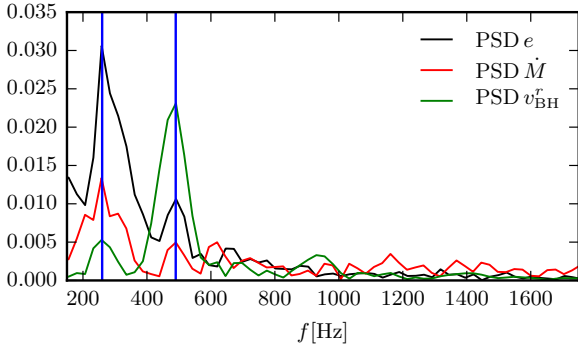


Figure 10. Power spectral densities of e , rest mass accretion rate \dot{M} , and radial BH velocity v_{BH}^r . The vertical lines indicate the 260 Hz and 490 Hz frequencies.

would mean that the QPOs we observe in the accretion rate would be at ~ 26 Hz and ~ 49 Hz if we rescale our results for a $10 M_{\odot}$ BH. These frequencies are compatible with the results of Machida & Matsumoto (2008), who found 10 Hz QPOs for a $10 M_{\odot}$ BH. Therefore, the QPOs we observe resulting from the modulation of the $m = 1$ mode strength could help explain the low-frequency QPO sector of the fast X-ray variability seen in LMXBs.

On the other hand, if we assume the accretor to be a NS, after rescaling our results for typical NS masses, the QPOs in the accretion rate would also have frequency peaks in a range compatible with those observed in LMXBs. Note that models based on the p -mode oscillations of axisymmetric tori cannot explain the observed twin QPOs in LMXBs with a NS as an accretor, with a fundamental frequency smaller than 500 Hz, since the fundamental mode frequency decreases as the size of the disc increases or as the distribution of the disc specific angular momentum approaches the Keplerian profile (Montero & Zanotti 2012). Therefore, the ω_1/f frequency ratio in axisymmetric models shows a tendency to concentrate towards the 3 : 2 ratio line as the fundamental mode frequency tends to zero. However, deviations from axisymmetry may relax this constraint, and there exist several works where the idea that the QPOs in accretion discs might be connected to non-axisymmetric modes has been put forward (see for instance Li et al. (2003); Tagger & Varnière (2006); Machida & Matsumoto (2008); Lai & Tsang (2009); Henisey et al. (2012)). By rescaling our results for a $1.4 M_{\odot}$ NS, the fundamental mode would lie at ~ 185 Hz while the first overtone would be at ~ 350 Hz. Such values, extracted from the modulation in the accretion rate triggered by the development of a non-axisymmetric $m = 1$ instability, lie thus within the range needed to explain, for instance, the observed QPOs in sources like Cir X-1 (Boutloukos et al. 2006) or XTE J1807-294 (Linares et al. 2005).

4 DISCUSSION

We have presented results from three-dimensional, numerical relativity simulations of a *tilted* black hole-thick accretion disc system. In particular, we have investigated in detail the BH-torus dynamics of one specific model, NC1a03b05, from the large set of models discussed in Mewes et al. (2016).

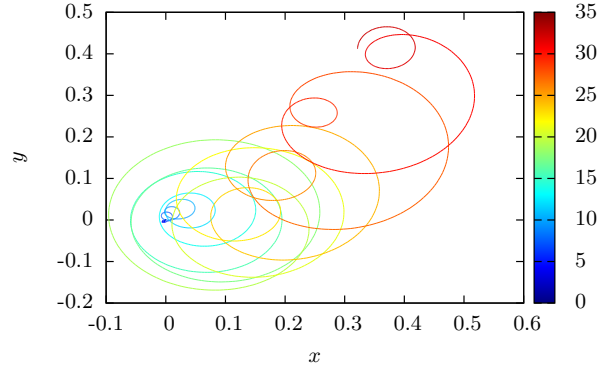


Figure 11. Trajectory of the BH projected onto the xy -plane. The colorbar indicates the time in t_{orb} along the trajectory.

In this paper we have employed fluid tracer particles as a powerful new tool to analyse the disc dynamics. The tracers provide a complementary tool to the existing disc analysis thorn described in Paper I.

Using the tracers, which accurately describe the bulk morphology of the fluid in the disc, we have shown that the BH precession we reported in Paper I is indeed caused by a torque resulting from the disc precessing as a solid body, which in turn results from the LT torque the BH exerts on the disc. This is expected, as the disc should exert an equal and opposite torque on the BH. For sufficiently high disc-to-BH mass ratios, tilted BH-torus systems should therefore contain precessing central BHs, and the BHs should precess for at least the accretion timescale of the disc.

The main characteristic of the BH-torus model considered is its non-constant specific angular momentum profile. As already observed in the numerical relativity simulations of Kiuchi et al. (2011) and in Paper I, these models form a long-lived over-density “planet” as the result of the growth of the $m = 1$ non-axisymmetric instability manifests itself as a spiral density wave of constant pattern speed in the differentially rotating disc. The pattern period has been shown to be slightly smaller than the initial fluid period at the location of the maximum rest-mass density of the disc. While the spiral wave remains of small amplitude, it travels through the fluid without interaction. Once the wave amplitude becomes large enough for non-linear effects to become important (in some regions the fractional change in rest-mass density becomes as high as 0.9), the wave couples to the fluid via the formation of mild shocks, which can be seen clearly as an increase in the fluid entropy. As the disc is differentially rotating, the spiral density wave has *negative* angular momentum w.r.t. the fluid inside the so-called corotation radius; therefore, the wave can transport fluid angular momentum outwards and becomes the main driver for accretion.

The density wave also represents a time-changing non-axisymmetric gravitational potential. As observed in Koberkin et al. (2011) and Paper I, this gravitational potential causes the BH to move along a spiral trajectory. Using the tracers, we have calculated the total gravitational pull exerted by the disc on the BH and have shown that the resulting torque agrees very well with the observed motion of the BH. This is an important confirmation that the BH motion

is of physical origin, and not caused by numerical effects or the evolution of the gauge variables lapse and shift. BH–disc alignment within the accretion timescale was observed in the numerical relativity simulations of tilted post-merger discs in [Kawaguchi et al. \(2015\)](#). Correspondingly, in the simulations reported in Paper I and in this work we have also seen partial realignment of the BH–torus system. In all cases, there was no explicit viscosity in the fluid evolution. As the torque acting to align the BH spin with the disc must be of dissipative nature, the only way to achieve BH–torus alignment is via numerical dissipation or dissipation via shocks in the fluid. The spiral density wave that results from the growth of the $m = 1$ mode provides such a channel, and [Kawaguchi et al. \(2015\)](#) have speculated that shocks in non-axisymmetric waves might be responsible for the observed alignment of the system. This is a strong argument to carefully check for non-axisymmetric structures in post-merger disks, as they seem to influence the evolution of BH–torus systems significantly.

Our simulations have also revealed the presence of distinct QPOs in the evolution of the accretion rate, in a frequency range compatible with that of X-ray luminosity QPOs in LMXBs. When rescaling the frequency of the observed QPOs in our simulation for a $10M_{\odot}$ BH, the extracted frequencies are compatible with the range of low-frequency QPOs in those systems. Furthermore, the same rescaling for typical NS masses also gives QPOs with frequencies compatible with those observed in sources like Cir X-1 or XTE J1807-294. The frequency ratio of the dominant low frequency peak and the first overtone found in our three-dimensional simulations is $\omega_1/f \sim 1.9$, a frequency ratio not attainable when modelling the QPOs as p -mode oscillations in axisymmetric tori. As the flow needs to develop a non-zero radial velocity component in order to accrete, we have also analysed the sum of disc eccentricity and ellipticity using the tracers and we have shown that its evolution exhibits the same QPO structure at exactly the same frequencies. While the origin of the variability of the eccentricity (which is also exhibited in the radial motion of the BH) is still unclear, the fact that the accretion rate is so clearly modulated could be the starting point to devise a new model to explain the observed QPOs in LMXBs.

ACKNOWLEDGEMENTS

Research supported by the Spanish Ministry of Economy and Competitiveness (MINECO) through grant AYA2013-40979-P, by the Generalitat Valenciana (PROMETEOII-2014-069), by the Max Planck Institute for Astrophysics, and by the Helmholtz International Center for FAIR within the framework of the LOEWE program launched by the State of Hesse. FG would like to thank David Radice for the useful discussions and for the help with the implementation of the tracer particles.

REFERENCES

Abramowicz M. A., Kluźniak W., McClintock J. E., Remillard R. A., 2004, *ApJ*, **609**, L63
 Adams F. C., Ruden S. P., Shu F. H., 1989, *Astrophys. J.*, **347**, 959

Alcubierre M., Brügmann B., Diener P., Koppitz M., Pollney D., Seidel E., Takahashi R., 2003, *Phys. Rev. D*, **67**, 084023
 Alic D., Rezzolla L., Hinder I., Mösta P., 2010, *Classical and Quantum Gravity*, **27**, 245023
 Baiotti L., Hawke I., Montero P. J., Löffler F., Rezzolla L., Stergioulas N., Font J. A., Seidel E., 2005, *Phys. Rev. D*, **71**, 024035
 Balbus S. A., Hawley J. F., 1991, *Astrophys. J.*, **376**, 214
 Bardeen J. M., Petterson J. A., 1975, *Astrophys. J.*, **195**, L65
 Baumgarte T. W., Shapiro S. L., 1998, *Phys. Rev. D*, **59**, 024007
 Belloni T. M., Stella L., 2014, *Space Science Reviews*, **183**, 43
 Blaes O. M., 1987, *Mon. Not. R. Astron. Soc.*, **227**, 975
 Boutloukos S., van der Klis M., Altamirano D., Klein-Wolt M., Wijnands R., Jonker P. G., Fender R. P., 2006, *Astrophys. J.*, **653**, 1435
 Brown D., Diener P., Sarbach O., Schnetter E., Tiglio M., 2009, *Phys. Rev. D*, **79**, 044023
 Campanelli M., Lousto C. O., Zlochower Y., Krishnan B., Merritt D., 2007, *Phys. Rev. D*, **75**, 064030
 Chandrasekhar S., 1960, *Proceedings of the National Academy of Science*, **46**, 253
 Christodoulou D. M., Narayan R., 1992, *Astrophys. J.*, **388**, 451
 Demianski M., Ivanov P. B., 1997, *Astron. Astrophys.*, **324**, 829
 Dreyer O., Krishnan B., Shoemaker D., Schnetter E., 2003, *Phys. Rev. D*, **67**, 024018
 Farris B. D., Duffell P., MacFadyen A. I., Haiman Z., 2014, *Astrophys. J.*, **783**, 134
 Foucart F., Duez M. D., Kidder L. E., Teukolsky S. A., 2011, *Phys. Rev. D*, **83**, 024005
 Foucart F., et al., 2013, *Phys. Rev. D*, **87**, 084006
 Foucart F., et al., 2014, *Phys. Rev. D*, **90**, 024026
 Fragile P. C., Anninos P., 2005, *Astrophys. J.*, **623**, 347
 Fragile P. C., Mathews G. J., Wilson J. R., 2001, *Astrophys. J.*, **553**, 955
 Fragile P. C., Blaes O. M., Anninos P., Salmonson J. D., 2007, *Astrophys. J.*, **668**, 417
 Fu W., Lai D., 2011, *Mon. Not. R. Astron. Soc.*, **410**, 1617
 Generozov A., Blaes O., Fragile P. C., Henisey K. B., 2014, *Astrophys. J.*, **780**, 81
 Gold R., Brügmann B., 2013, *Phys. Rev. D*, **88**, 064051
 Goodman J., Rafikov R. R., 2001, *Astrophys. J.*, **552**, 793
 Goodman J., Narayan R., Goldreich P., 1987, *Mon. Not. R. Astron. Soc.*, **225**, 695
 Hawley J. F., 1987, *Mon. Not. R. Astron. Soc.*, **225**, 677
 Hawley J. F., 1991, *Astrophys. J.*, **381**, 496
 Heemskerk M. H. M., Papaloizou J. C., Savonije G. J., 1992, *Astron. Astrophys.*, **260**, 161
 Heinemann T., Papaloizou J. C. B., 2012, *Mon. Not. R. Astron. Soc.*, **419**, 1085
 Henisey K. B., Blaes O. M., Fragile P. C., 2012, *Astrophys. J.*, **761**, 18
 Ivanov P. B., Illarionov A. F., 1997, *Mon. Not. R. Astron. Soc.*, **285**, 394
 Kawaguchi K., Kyutoku K., Nakano H., Okawa H., Shibata M., Taniguchi K., 2015, *Phys. Rev. D*, **92**, 024014
 Kidder L. E., 1995, *Phys. Rev. D*, **52**, 821
 King A. R., Lubow S. H., Ogilvie G. I., Pringle J. E., 2005, *Mon. Not. R. Astron. Soc.*, **363**, 49
 Kiuchi K., Shibata M., Montero P. J., Font J. A., 2011, *Physical Review Letters*, **106**, 251102
 Korobkin O., Abdikamalov E. B., Schnetter E., Stergioulas N., Zink B., 2011, *Phys. Rev. D*, **83**, 043007
 Kozai Y., 1962, *AJ*, **67**, 591
 Lai D., Tsang D., 2009, *Mon. Not. R. Astron. Soc.*, **393**, 979
 Lense J., Thirring H., 1918, *Physikalische Zeitschrift*, **19**
 Li L.-X., Goodman J., Narayan R., 2003, *Astrophys. J.*, **593**, 980
 Lidov M. L., 1962, *Planet. Space Sci.*, **9**, 719

- Linares M., van der Klis M., Altamirano D., Markwardt C. B., 2005, *Astrophys. J.*, 634, 1250
- Löffler F., et al., 2012, *Classical and Quantum Gravity*, 29, 115001
- Lubow S. H., Ogilvie G. I., Pringle J. E., 2002, *Mon. Not. R. Astron. Soc.*, 337, 706
- MacFadyen A. I., Milosavljević M., 2008, *Astrophys. J.*, 672, 83
- Maccarone T. J., 2002, *Mon. Not. R. Astron. Soc.*, 336, 1371
- Machida M., Matsumoto R., 2008, *PASJ*, 60, 613
- Martin R. G., Nixon C., Lubow S. H., Armitage P. J., Price D. J., Doğan S., King A., 2014, *ApJ*, 792, L33
- Masset F., Tagger M., 1997, *Astron. Astrophys.*, 322, 442
- Mazur G. P., Zanutti O., Sądowski A., Mishra B., Kluźniak W., 2016, *Mon. Not. R. Astron. Soc.*, 456, 3245
- Méndez M., van der Klis M., Ford E. C., Wijnands R., van Paradijs J., 1999, *ApJ*, 511, L49
- Merritt D., Vasiliev E., 2012, *Phys. Rev. D*, 86, 102002
- Mewes V., Font J. A., Montero P. J., 2015, *Phys. Rev. D*, 91, 124043
- Mewes V., Font J. A., Galeazzi F., Montero P. J., Stergioulas N., 2016, *Phys. Rev. D*, 93, 064055
- Mishra B., Vincent F. H., Manousakis A., Fragile P. C., Paumard T., Kluźniak W., 2015, preprint, ([arXiv:1510.07414](https://arxiv.org/abs/1510.07414))
- Montero P. J., Zanutti O., 2012, *Mon. Not. R. Astron. Soc.*, 419, 1507
- Mösta P., et al., 2014, *Classical and Quantum Gravity*, 31, 015005
- Nakamura K., Kajino T., Mathews G. J., Sato S., Harikae S., 2015, *Astron. Astrophys.*, 582, A34
- Nealon R., Nixon C., Price D. J., King A., 2016, *Mon. Not. R. Astron. Soc.*, 455, L62
- Nelson R. P., Papaloizou J. C. B., 2000, *Mon. Not. R. Astron. Soc.*, 315, 570
- Papaloizou J. C. B., Lin D. N. C., 1995, *Annu. Rev. Astron. Astrophys.*, 33, 505
- Papaloizou J. C. B., Pringle J. E., 1984, *Mon. Not. R. Astron. Soc.*, 208, 721
- Rees M. J., 1978, *Nature*, 275, 516
- Reisswig C., Ott C. D., Sperhake U., Schnetter E., 2011, *Phys. Rev. D*, 83, 064008
- Rezzolla L., Yoshida S., Maccarone T. J., Zanutti O., 2003, *Mon. Not. R. Astron. Soc.*, 344, L37
- Roedig C., Sesana A., Dotti M., Cuadra J., Amaro-Seoane P., Haardt F., 2012, *Astron. Astrophys.*, 545, A127
- Scheuer P. A. G., Feiler R., 1996, *Mon. Not. R. Astron. Soc.*, 282, 291
- Schnetter E., Hawley S. H., Hawke I., 2004, *Classical and Quantum Gravity*, 21, 1465
- Schnetter E., Krishnan B., Beyer F., 2006, *Phys. Rev. D*, 74, 024028
- Shibata M., Nakamura T., 1995, *Phys. Rev. D*, 52, 5428
- Tagger M., Varnière P., 2006, *Astrophys. J.*, 652, 1457
- Thornburg J., 2003, in Centrella J. M., ed., *American Institute of Physics Conference Series Vol. 686, The Astrophysics of Gravitational Wave Sources*. pp 247–252, [doi:10.1063/1.1629439](https://doi.org/10.1063/1.1629439)
- Travaglio C., Hillebrandt W., Reinecke M., Thielemann F.-K., 2004, *Astron. Astrophys.*, 425, 1029
- Velikhov E., 1959, *Zhur. Eksptl'. i Teoret. Fiz.*, 36
- Zhou X.-L., Yuan W., Pan H.-W., Liu Z., 2015, *ApJ*, 798, L5
- Zurek W. H., Benz W., 1986, *Astrophys. J.*, 308, 123
- van Paradijs J., Penninx W., Lewin W. H. G., 1988, *Mon. Not. R. Astron. Soc.*, 233, 437
- van der Klis M., 2006, in Lewin W., van der Klis M., eds, *Compact Stellar X-Ray Sources*. Cambridge University Press, pp 39–112